Review Article

Mitochondrial-Targeted Two-Photon Fluorescent Probes for Zinc Ions, H_2O_2, and Thiols in Living Tissues

Hwan Myung Kim[1] and Bong Rae Cho[2]

[1] *Division of Energy Systems Research, Ajou University, Suwon 443-749, Republic of Korea*
[2] *Department of Chemistry, Korea University, 1-Anamdong, Seoul 136-701, Republic of Korea*

Correspondence should be addressed to Hwan Myung Kim; kimhm@ajou.ac.kr and Bong Rae Cho; chobr@korea.ac.kr

Mitochondria provide the energy of the cells and are the primary site of oxygen consumption and the major source of reactive oxygen species. In mitochondria, metal ions and glutathione play vital roles in maintaining their structure and the redox environment. To understand their roles in mitochondria, it is crucial to monitor each of these chemical species in the mitochondria at the cell, tissue, and organism levels. An ideal tool for such purpose is the use of two-photon microscopy (TPM). Until recently, however, there has been no report on the two-photon (TP) probes suitable for such applications. In this paper, we summarize the mitochondria-targeted TP probes for Zn^{2+}, H_2O_2, and thiols, as well as their bioimaging applications.

1. Introduction

Mitochondria provide the energy of the cells. They are primary cellular compartments of oxygen consumption and the major source of reactive oxygen species (ROS) [1, 2]. In mitochondria, metal ions and glutathione (GSH) play vital roles in maintaining their structure and the redox environment [3–6]. To understand the physiology of mitochondria, it is crucial to monitor such chemical species in mitochondria at the cell, tissue, and organism levels. For this purpose, a number of one-photon fluorescent probes, derived from fluorescein or rhodamine as the fluorophore and various receptors, have been developed [7–9]. However, most of these probes have been evaluated with one-photon microscopy (OPM), which uses single photon of higher energy as the excitation source (Scheme 1(a)). This requirement limited their application in live tissue imaging owing to the shallow penetration depth (less than $80\,\mu$m), photobleaching, and cellular autofluorescence.

An attractive approach to the detection of biologically important species deep inside live tissues is the use of two-photon microscopy (TPM). TPM, a new technique which employs two near-infrared photons as the excitation source (Scheme 1(a)), has become an indispensable tool in biology

and medicine due to the advantages it offers. They include deeper penetration depth ($>500\,\mu$m), lower tissue auto-fluorescence and self-absorption, reduced photodamage and photobleaching, in addition to the intrinsically localized excitation [13–16]. This allows molecular imaging deep inside the intact tissue for a long period of time with minimum interference from the tissue preparation artifacts which can extend $>70\,\mu$m into the tissue interior [17]. However, the progress in this field is limited by the lack of two-photon (TP) probes. As such, many biologists are using one photon fluorescent probes for TPM imaging, despite that most of them have too low two-photon (TP) cross-sections ($\delta_{\text{TPA}} < 50\,$GM) to be useful for TPM [18]. Therefore, there is a pressing need to develop a variety of TP probes for specific applications [15, 16].

To meet such demands, we have developed a series of mitochondrial-targeted TP probes that can selectively detect mitochondrial Zn^{2+} (SZn-Mito, SZn2-Mito), H_2O_2 (SHP-Mito), and thiols (SSH-Mito) in live tissues (Scheme 1(c)) [10–12, 19]. These probes are derived from 6-(benzo[d]thiazol-2$'$-yl)-2-(N,N-dimethylamino)naphthalene (BT-DAN) as the TP fluorophore, triphenylphosphonium salt (TPP) as the mitochondrial targeting site [20, 21], and
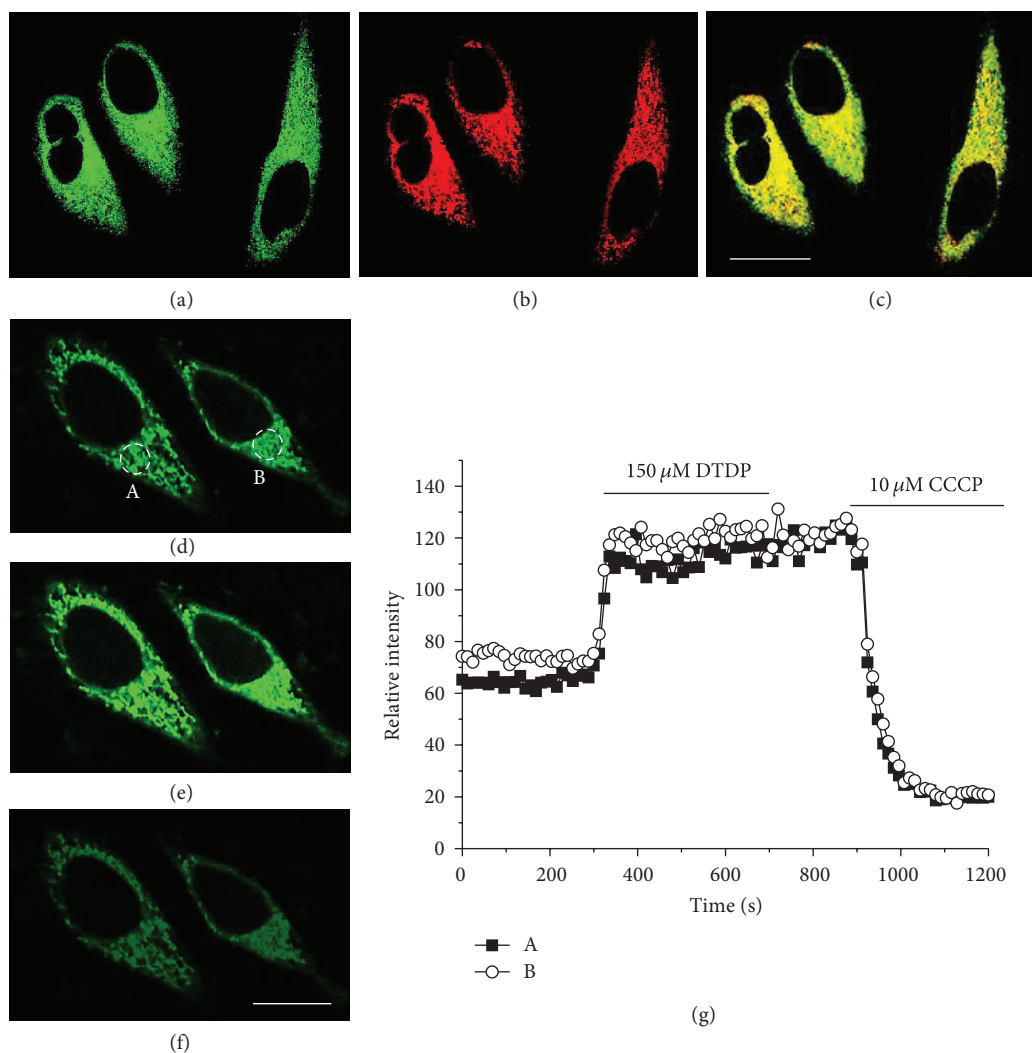
Figure 1: (a) TPM and (b) OPM images of HeLa cells colabeled with (a) SZn2-Mito (1 μM) and (b) Mitotracker Red FM (1 μM). (c) Colocalized image. The wavelengths for one- and two-photon excitations were 514 and 760 nm, respectively, and the emission was collected at 450–550 (SZn-Mito) and 600–700 nm (Mitotracker Red FM), respectively. Scale bar, 20 μm. (d–f) TPM images of 1 μM SZn2-Mito-labeled HeLa cells, before (d) and after (e) addition of 150 μM DTDP to the imaging solution. (f) After addition of 10 μM CCCP to (e). (g) The relative TPEF intensity of SZn2-Mito-labeled HeLa cells as a function of time. The TPEF intensities were collected at 450–600 nm upon excitation at 750 nm with fs pulse. Scale bar, 10 μm. Cells shown are representative images from replicate experiments ($n = 5$) [10].

receptors for the specific analytes (Scheme 1(b)). TPP and the receptors have been separated as far as possible to minimize the interactions between them. In this paper, we summarize the photophysical properties and biological imaging applications of mitochondrial-targeted TP probes for Zn^{2+}, H_2O_2, and thiols.

2. Two-Photon Probes for Mitochondrial Zinc Ion

Zinc ion is the second most abundant d-block metal ion in the human brain and is an active component in enzymes and proteins [22–26]. For proper brain functions, it is vital to maintain Zn^{2+}-ion homeostasis, which is controlled by the import of intracellular free Zn^{2+} ions ($[Zn^{2+}]_i$) from and export to

the extracellular cellular space, the endoplasmic reticulum, and mitochondria. While mitochondria can take up evoked $[Zn^{2+}]_i$ rise, a strong elevation of intramitochondrial Zn^{2+} ($[Zn^{2+}]_m$) can promote mitochondrial dysfunctions [27, 28]. Recently, we have developed TP probes for $[Zn^{2+}]_m$ (SZn-Mito and SZn2-Mito, Scheme 1(c)) derived from BTDAN as the reporter, N,N-di-(2-picolyl)ethylenediamine (DPEN) as the Zn^{2+} chelator, [29, 30] and TPP as the mitochondrial targeting group.

SZn-Mito and SZn2-Mito are TP fluorescent turn-on probes based on the photoinduced electron transfer (PeT) process [31]. Upon addition of Zn^{2+}, the fluorescence intensity of SZn-Mito and SZn2-Mito increased gradually presumably because of the blocking of the PeT upon binding with Zn^{2+}. The TP fluorescence enhancement factor (FEF =
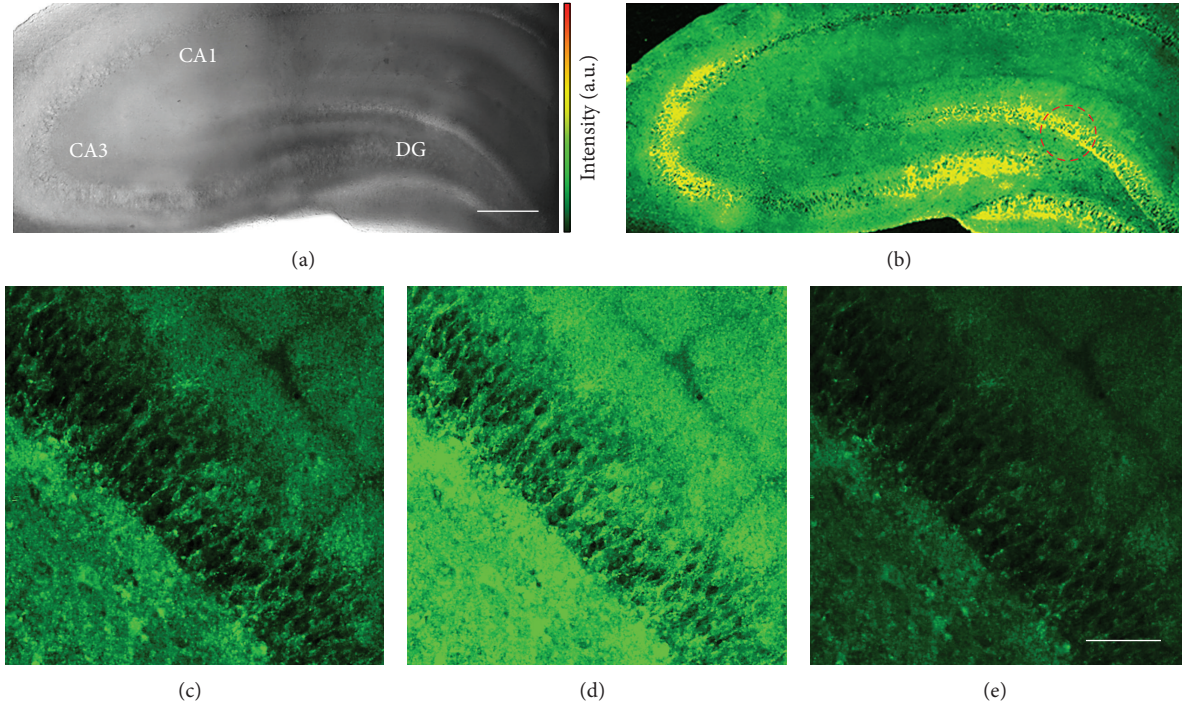
FIGURE 2: Images of a rat hippocampal slice stained with 20 μM SZn2-Mito for 1 h. (a) Bright-field images of the CA1-CA3 regions as well as dentate gyrus (DG) at 10x magnification. (b) 10 TPM images along the z-direction at the depths of approximately 100–200 μm were accumulated. (c–e) Magnification at 40x in the DG regions (red circle in (b)) at a depth of ~100 μm (c) before and (d) after addition of 150 μM DTDP to the imaging solution. (e) After addition of 10 μM CCCP to (d). Scale bars: (a) 300 and (e) 75 μm [10].

TABLE 1: Photophysical data for TP probes [10–12, 19].

Probe	$\lambda^{(1)}_{max}/\lambda^{fl}_{max}$ [a]	Φ [b]	K_d^{OP}/K_d^{TP} [c]	FEF [d]	R_{max}/R_{min} [e]	$\lambda^{(2)}_{max}$ [f]	$\delta\Phi$ [g]
SZn-Mito [h]	388/500	0.15	3.1/3.1 nM	7 (7)	—	—	—
SZn-Mito/Zn^{2+} [h]	375/493	0.92				760	75
SZn2-Mito [i]	413/536	0.0048	1.4/1.4 nM	70 (68)	—	—	—
SZn2-Mito/Zn^{2+} [i]	395/536	0.33				750	155
SSH-Mito [j]	338/462	0.82	—	—	45(40)	740	80
SSH-Mito/GSH (1-SSH) [j]	383/545	0.12				750	55
SHP-Mito [k]	342/470	0.13	—	—	75(40)	740	11
SHP-Mito/H$_2$O$_2$ (1-SHP) [k]	383/545	0.12				750	55

[a] λ_{max} of the one-photon absorption and emission spectra in nm. [b] Fluorescence quantum yield. [c] Dissociation constants measured by one- (K_d^{OP}) and two-photon (K_d^{TP}) processes, except otherwise noted. [d] Fluorescence enhancement factor, $(F - F_{min})/F_{min}$, measured by one-photon processes. The number in parentheses is measured by two-photon process. [e] R_{max} and R_{min} represent the maximum and minimum ratios of F_{yellow}/F_{blue}, where F_{yellow} and F_{blue} are the fluorescence intensities measured at 425–475 nm (F_{blue}) and 525–575 nm (F_{yellow}), respectively. The number in parentheses was measured by two-photon process. [f] λ_{max} of the two-photon excitation spectra in nm. [g] The peak two-photon action cross-section in 10^{-50} cm^4 s/photon (GM). [h] Measured in MOPS buffer (30 mM MOPS, 100 mM KCl, 10 mM EGTA, pH 7.2) in the absence and presence (120 nM) of free Zn^{2+}. [i] Measured in HEPES buffer (50 mM HEPES, 100 mM KCl, 10 mM NTA, pH 7.4) in the absence and presence (47 nM) of free Zn^{2+}. [j] Measured in MOPS buffer (30 mM MOPS, 100 mM KCl, pH 7.4) before and 2 h after addition of 10 mM GSH. [k] Measured in MOPS buffer (30 mM MOPS, 100 mM KCl, pH 7.4) before and 1 h after addition of 1 mM H$_2$O$_2$.

$(F - F_{min})/F_{min})$ of SZn-Mito was 7 in MOPS buffer (30 mM, pH 7.2), while that of SZn2-Mito was 68 in HEPES buffer (50 mM, pH 7.4) (Table 1) [10]. Noteworthy was the large (10-fold) increase in the FEF by the slight modification of the chemical structure. The dissociation constants (K_d^{OP} and K_d^{TP}) of SZn-Mito and SZn2-Mito for the complexation with Zn^{2+} were 3.1 and 1.4 nM, respectively, regardless of the

excitation mode (Table 1); thus, these probes can detect Zn^{2+} in the nanomolar range. Both probes exhibited high selectivity for 1 μM Zn^{2+} compared with 1 mM of Na$^+$, K$^+$, Ca^{2+}, Mg^{2+}, 1 μM of Mn^{2+}, Fe^{2+}, Co^{2+}, and Pb^{2+} and modest selectivity over 1 μM Ni^{2+} and Cd^{2+} [10, 19]. In the presence of 1 μM of Cu^{2+} and Hg^{2+}, the fluorescence was quenched due to the metal-to-ligand electron transfer upon excitation
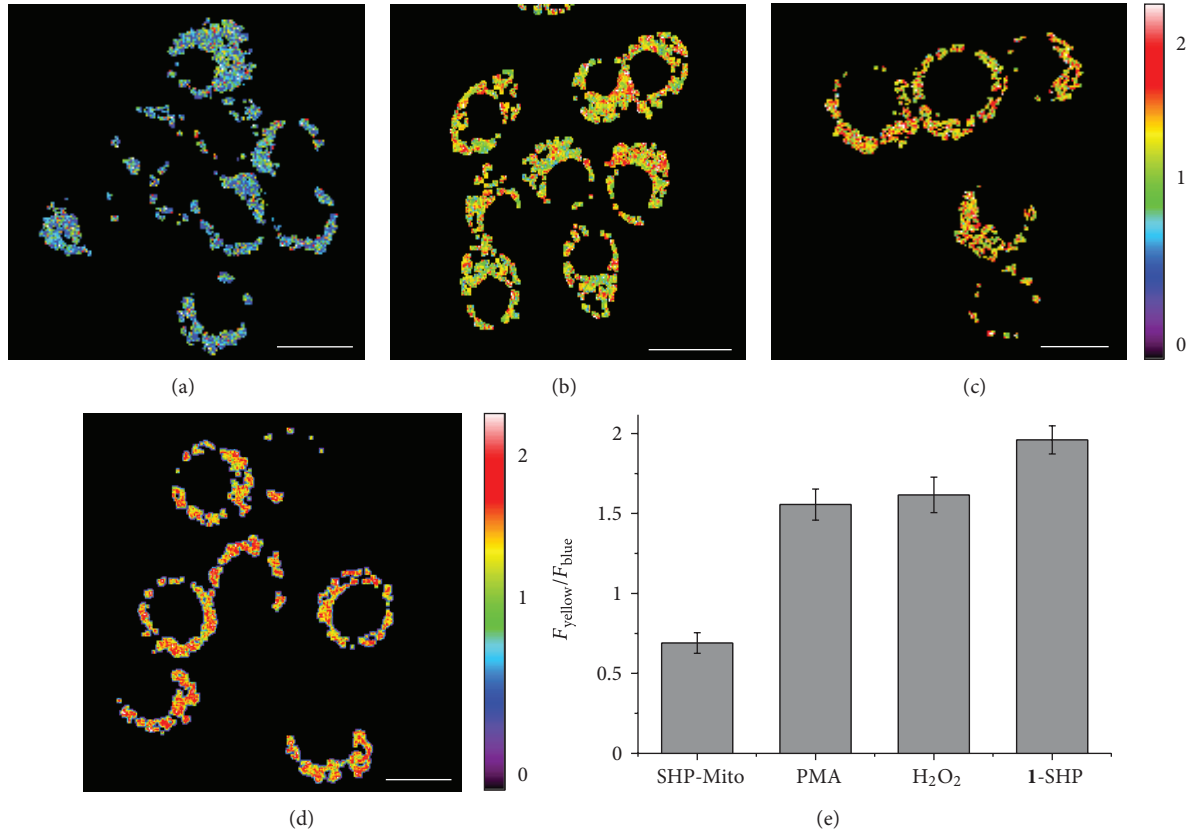
FIGURE 3: (a–d) Pseudocolored ratiometric TPM images ($F_{\text{yellow}}/F_{\text{blue}}$) of Raw 264.7 cells incubated with 3 μM (a) SHP-Mito and (d) **1**-SHP. (b and c) Cells were pretreated with (b) PMA (1 μg/mL) for 30 min and (c) 200 μM H_2O_2 for 30 min. (e) Average $F_{\text{yellow}}/F_{\text{blue}}$ intensity ratios in figures (a–d). Images were acquired using 750 nm excitation and fluorescent emission windows: blue = 400–470 nm and yellow = 530–600 nm. Scale bar = 15 μm. Cells shown are representative images from replicate experiments (n = 5) [11].

[32]. Moreover, they were pH insensitive in the biologically relevant pH range. Since Ni^{2+}, Cd^{2+}, Hg^{2+}, and Cu^{2+} ions rarely exist in the cells [33], these probes can detect Zn^{2+} with minimum interference from other competing metal ions and pH. Moreover, the TP action cross-sections ($\Phi\delta$) of SZn-Mito and SZn2-Mito were 75 and 155 GM at 760 and 750 nm, respectively, in the presence of excess Zn^{2+} (Table 1). The combined results reveal that SZn2-Mito is a more sensitive TP probe which can detect mitochondrial Zn^{2+} with higher sensitivity and twice as bright TPM image than SZn-Mito.

The utility of SZn2-Mito in the cell imaging was confirmed by the following experiments. First, the TPM and OPM images of HeLa cells colabeled with SZn2-Mito and Mitotracker Red FM, a well-known OP fluorescent probe for mitochondria [8], overlapped well. The Pearson's colocalization coefficient, A, calculated by using Autoquant X2 software, of SZn2-Mito with Mitotracker Red FM was 0.85 (Figures 1(a)–1(c)) [34]. Second, the TPEF intensity decreased dramatically when the probe-labeled cells were treated with N,N,N',N'-tetrakis(2-pyridyl)ethylenediamine (TPEN), a membrane permeable Zn^{2+} chelator that can effectively remove $[Zn^{2+}]_m$ [35]. Third, SZn2-Mito showed negligible toxicity as measured by using CCK-8 kit and high photostability as indicated by the negligible change in the

TP excited fluorescence (TPEF) intensity after continuous irradiation of the fs pulses for 60 min [10]. Fourth, the TPEF intensity increased dramatically when 2,2'-dithiodipyridine (DTDP; 150 μM), a reagent that promotes the release of Zn^{2+} from Zn^{2+}-binding proteins [36], was added to HeLa cells labeled with SZn2-Mito (Figures 1(d), 1(e), and 1(g)) and decreased abruptly upon addition of carbonyl cyanide m-chlorophenylhydrazone (CCCP; 10 μM, Figures 1(f) and 1(g)), a compound that promotes the release of intramitochondrial cations by collapsing the mitochondrial membrane potential [37].

To assess the utility of SZn2-Mito in tissue imaging, fresh hippocampal slices from a 14-day-old rat were labeled with 20 μM SZn2-Mito. The TPM image of the probe-labeled tissue revealed marked TPEF in the CA3 and DG regions at depths of 100–200 μm (Figure 2(b)). At a higher magnification, the $[Zn^{2+}]_m$ distribution in the DG region was clearly visualized (Figure 2(c)). Moreover, the TPEF intensity increased after addition of DTDP and decreased upon treatment of CCCP, thereby confirming that the bright regions reflect the $[Zn^{2+}]_m$ (Figures 2(d) and 2(e)). These results established that SZn2-Mito is capable of detecting $[Zn^{2+}]_m$ at depths of 100–200 μm in living tissues by using TPM [10].
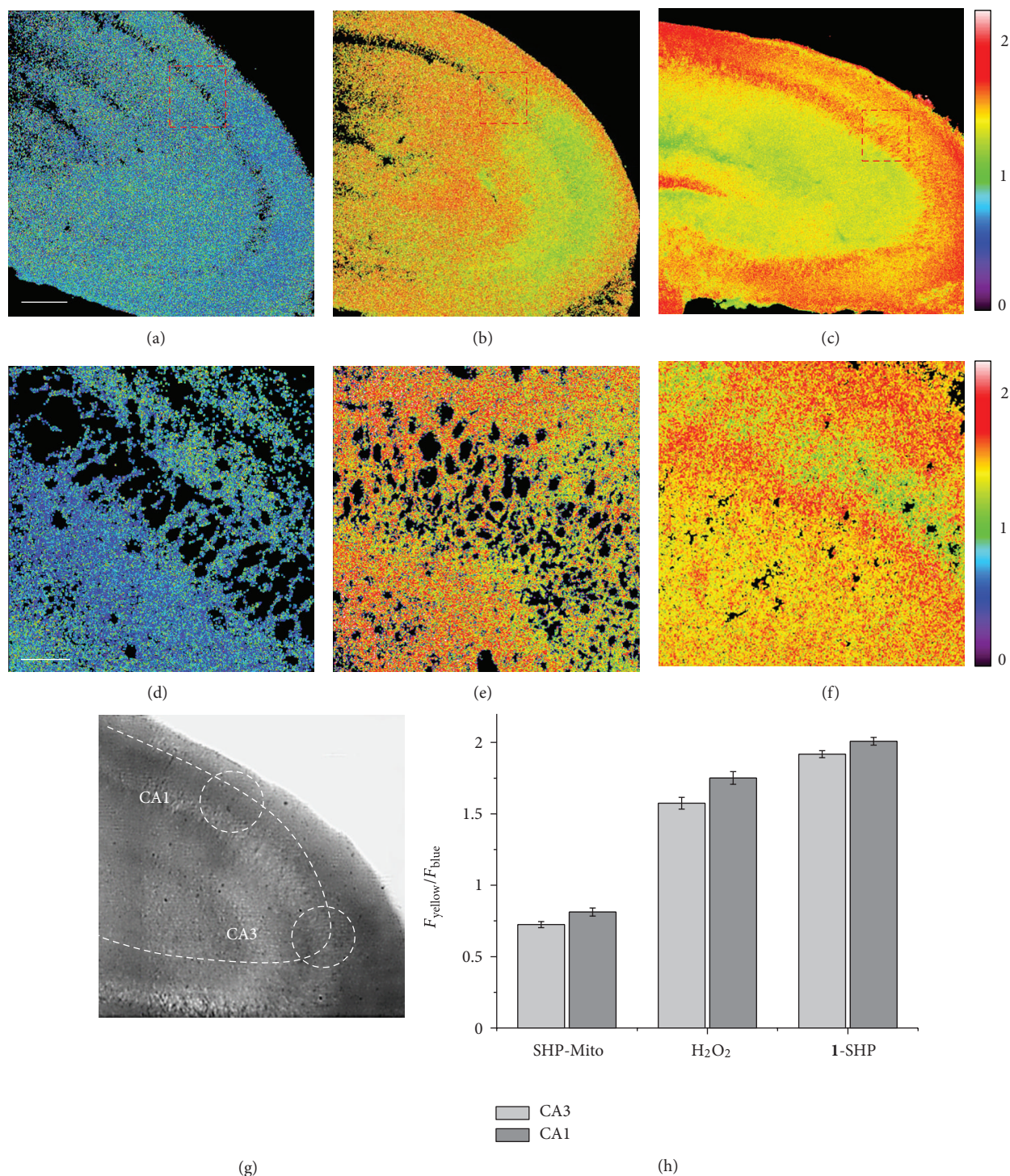
Figure 4: Ratiometric TPM images of a rat hippocampal slice stained with (a) 20 μM SHP-Mito and (c) **1**-SHP and (b) pretreated with 1 mM H_2O_2 for 30 min before labeling with 20 μM SHP-Mito. Ten ratiometric TPM images were accumulated along the z-direction at the depths of approximately 90–180 μm with magnification at 10x. (d–f) Enlarged images of (a–c) at 120 μm depth with 40x magnification. (g) Approximate positions (dotted circles) used for measurements of emission ratios in the CA3 and CA1. (h) Average F_{yellow}/F_{blue} in (a–c). The TPEF was collected at two channels (blue = 400–470 nm and yellow = 530–600 nm) upon excitation at 750 nm with fs pulse. Scale bars: 300 μm (a) and 75 μm (d) [11].
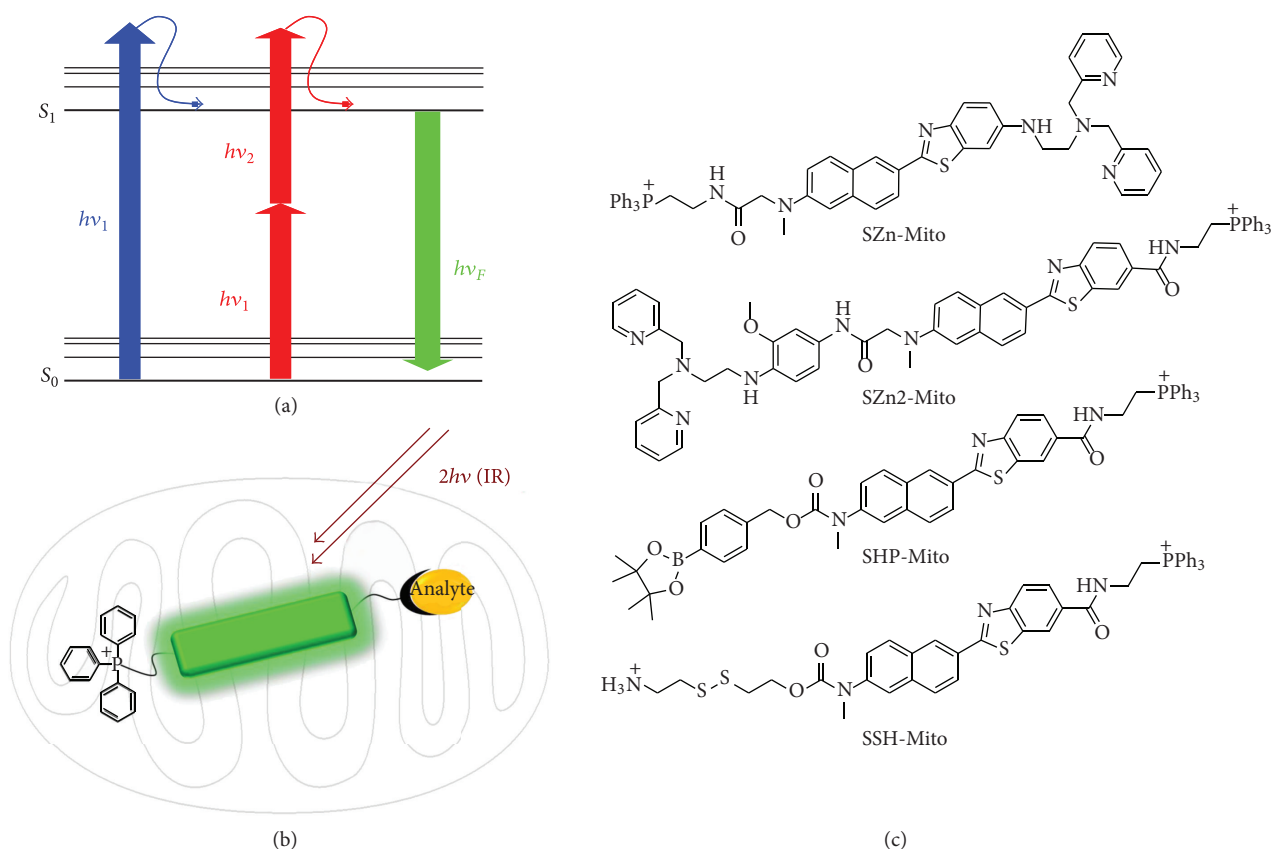
SCHEME 1: (a) Comparison of one- and two-photon exited fluorescence; the fluorescence is emitted upon excitation by one-photon of higher energy and two-photons of lower energy, respectively. (b) Design of the mitochondria-targeted two-photon probes. Mitochondrial targeting moiety (TPP) and receptors for the analytes are linked to the opposite ends of the fluorophore. (c) Chemical structures of the mitochondrial-targeted two-photon probes for Zn^{2+} (SZn-Mito and SZn2-Mito), H_2O_2 (SHP-Mito), and thiols (SSH-Mito).
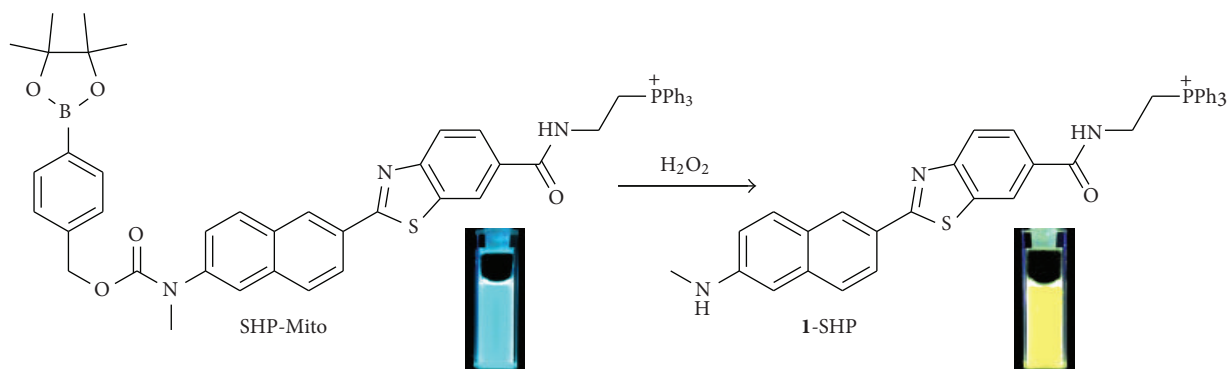

SCHEME 2: Structures of SHP-Mito and **1**-SHP [11].

3. Two-Photon Probe for Mitochondrial H_2O_2

Hydrogen peroxide (H_2O_2) is a prominent member of the ROS family and plays crucial roles in physiology, aging, and disease in living organisms [38–40]. While controlled bursts of H_2O_2 are utilized for cell signaling [41], abnormal production or accumulation of H_2O_2 within mitochondria has been linked to severe disorder such as cancer and neurodegenerative Alzheimer's and Parkinson's diseases [42–44]. To detect mitochondrial H_2O_2 deep inside live tissues, we have developed a ratiometric TP probe (SHP-Mito, Scheme 2) derived from BTDAN as the reporter, a boronate-based carbamate leaving group as the H_2O_2 response site, and TPP as the mitochondrial targeting site. We anticipated that
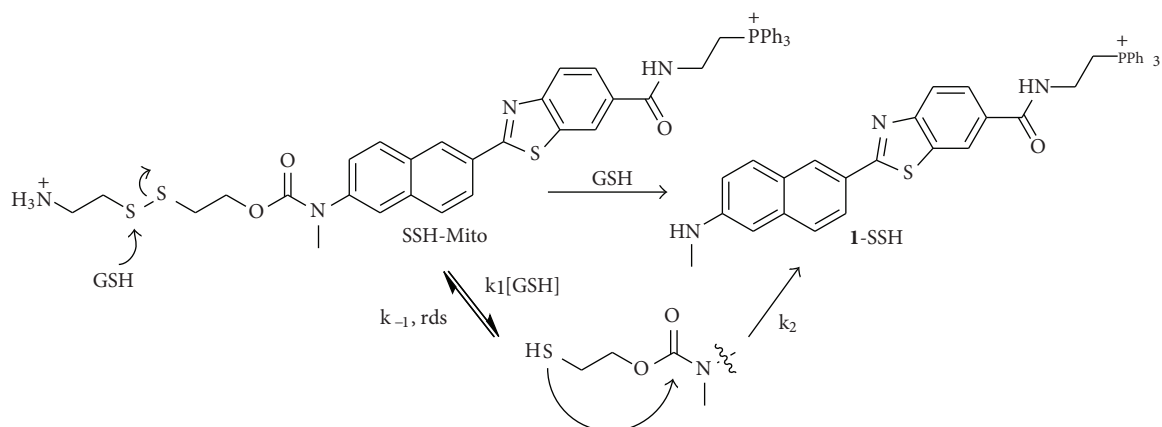
SCHEME 3: Structures of SSH-Mito and mechanism of the GSH-induced reduction of SSH-Mito [12].
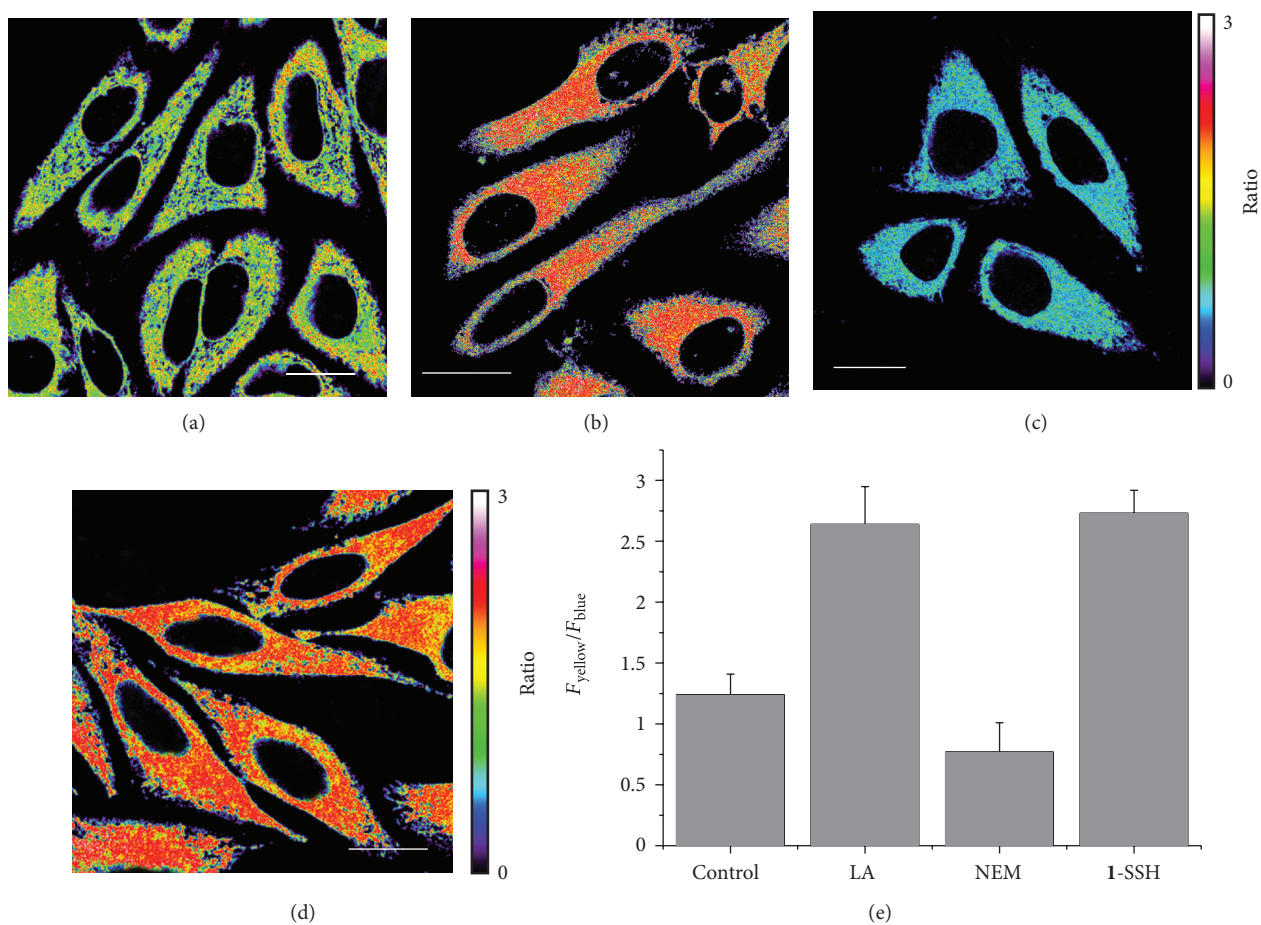

FIGURE 5: (a–d) Pseudocolored ratiometric TPM images (F_{yellow}/F_{blue}) of HeLa cells incubated with 5 μM SSH-Mito (a) and **1**-SSH (d) and pretreated with lipoic acid (500 μM) for 1 day (b) and NEM (100 μM) for 30 min (c) before labeling with SSH-Mito. (e) Average F_{yellow}/F_{blue} intensity ratios in figures (a–d). Images were acquired using 740 nm excitation and fluorescent emission windows: blue = 425–475 nm and yellow = 525–575 nm. Scale bar = 20 μm. Cells shown are representative images from replicate experiments ($n = 5$) [12].
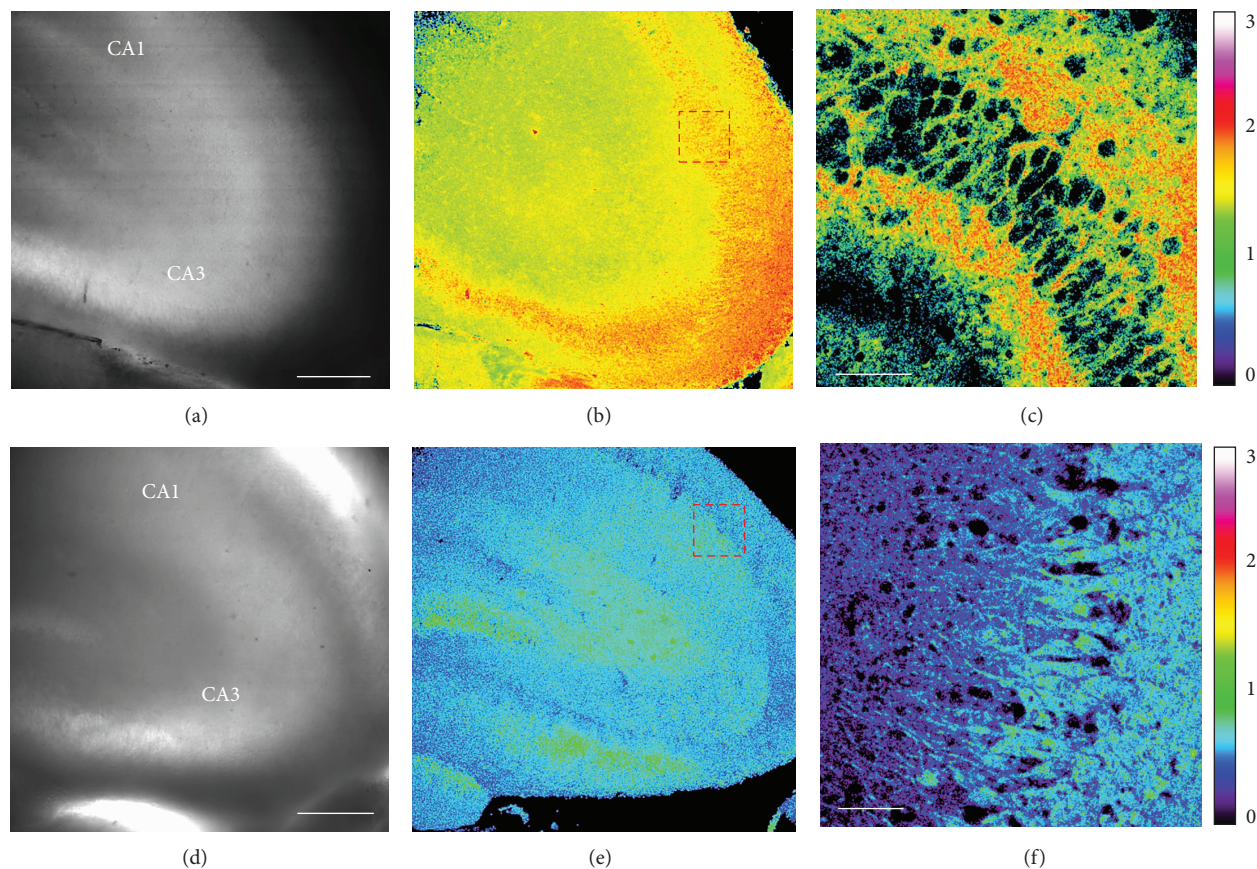
FIGURE 6: Images of a rat hippocampal slice stained with 20 μM SSH-Mito for 2 h. (a and d) Bright-field images of the CA1-CA3 regions. (b and e) Ratiometric TPM images of a fresh rat hippocampal slice (b) nontreated and (e) pretreated with NEM (100 μM) for 30 min before labeling with SSH-Mito. Ten ratiometric TPM images were accumulated along the z-direction at the depths of approximately 90–190 μm with magnification at 10x. (c and f) Enlarged images of red box in (b) and (e) at 120 μm depth with 40x magnification. The TPEF was collected at two channels (blue = 425–475 nm and yellow = 525–575 nm) upon excitation at 740 nm with fs pulse. Scale bars: 300 μm (a and d) and 75 μm (c and f) [12].

the H_2O_2-triggered boronate cleavage of the electron poor carbamate linkage would liberate the more electron rich **1**-SHP, giving rise to red-shifted fluorescent emission (Scheme 2) [11].

The emission spectra of a 1 μM solution of SHP-Mito increased gradually at 530–600 nm (F_{yellow}) with a concomitant decrease at 400–470 (F_{blue}) nm in the presence of 1 mM H_2O_2 in MOPS buffer [11]. This process followed pseudo 1st-order kinetics with $k_{obs} = 1.0$–1.2×10^{-3} s^{-1} and resulted in a 75-fold enhancement in the F_{yellow}/F_{blue} ratio. The detection limit of SPH-Mito for H_2O_2 was 4.6 μM. Moreover, SHP-Mito exhibited high selectivity for H_2O_2 over competing ROS and reactive nitrogen species (RNS), as revealed by unperturbed F_{yellow}/F_{blue} ratios upon addition of 200 μM concentrations of various ROS and RNS, including *tert*-butyl hydroperoxide (TBHP), hypochlorite (OCl$^-$), super-oxide (O$_2^-$), nitric oxide (NO), *tert*-butoxy radical ($^\bullet$OBu^t), hydroxyl radical ($^\bullet$OH), and peroxynitrite (ONOO$^-$), and was pH insensitive at biologically relevant pH range [11]. The TP action ($\Phi\delta$) spectra of SHP-Mito and **1**-SHP in MOPS

buffer (30 mM, pH 7.4) indicated $\Phi\delta_{max}$ values of 11 and 55 GM at 740 and 750 nm, respectively (Table 1). This predicts 5-fold brighter TPM images of the probe-labeled cells after complete conversion of SHP-Mito to **1**-SHP.

The utility of SHP-Mito in the live cell imaging was established by the following experiments. First, the TPM and OPM images of Raw 264.7 murine macrophage cells co-labeled with SHP-Mito and MitoTracker Red merged well with the A of 0.91 [11]. Second, the ratiometric images constructed from two collection windows ranging from 400 to 470 nm (F_{blue}) and 530 to 600 nm (F_{yellow}) gave an average emission ratio of $F_{yellow}/F_{blue} = 0.62$ and 1.96 for SHP-Mito and **1**-SHP, respectively (Figures 3(a), 3(d), and 3(e)). The ratio increased to 1.62 when the cells were preincubated for 30 min with 200 μM H_2O_2 and to 1.56 upon treatment with phorbol myristate acetate (PMA), which induces H_2O_2 generation through a cellular inflammation response (Figures 3(b), 3(c), and 3(e)) [45]. These results confirmed that SHP-Mito is responsive to the change in the H_2O_2 concentration. Third, SHP-Mito shows nontoxicity to cells during the imaging experiments, as determined by using a CCK-8 kit [11].

The utility of SHP-Mito in the tissue imaging was established by a similar protocol as described earlier. TPM image of fresh hippocampal slices from a 2-day-old rat labeled with $20\,\mu$M SHP-Mito revealed that H_2O_2 is more or less evenly distributed in both the CA1 (F_{green}/F_{blue} = 0.81) and CA3 (F_{green}/F_{blue} = 0.72) regions (Figure 4(a)) at depths of 90–$180\,\mu$m. Upon treatment of the tissue with increasing amounts of H_2O_2, the ratio increased gradually to 1.57 (CA3) and 1.75 (CA1) at $1\,$mM H_2O_2, which lie between those measured in SHP-Mito- and **1**-SHP-labeled tissues (Figure 4(h)). Hence, SHP-Mito is responsive to rises in H_2O_2 in tissue. Moreover, the ratiometric image at higher magnification clearly showed the H_2O_2 distribution in the individual cells in the CA3 region at a depth of $120\,\mu$m (Figures 4(d)–4(f)). Hence, SHP-Mito is capable of detecting mitochondrial H_2O_2 in live tissues using TPM [11].

4. Two-Photon Probe for Mitochondrial Thiols

Intracellular thiols such as cysteine (Cys), homocystein (Hcy), and glutathione (GSH) play vital roles in biology [3–5]. They maintain higher-order structures of proteins and control redox homeostasis through the equilibrium between thiols (RSH) and disulfides (RSSR) [46]. In mitochondria, GSH plays a key role in maintaining the redox environment to avoid or repair oxidative damage leading to dysfunction and cell death [47]. Mitochondrial GSH (mGSH) exists predominantly in the reduced form, with the GSH : GSSG ratio being greater than $100:1$ [48]. To detect GSH deep inside live tissues, we have developed a TP probe (SSH-Mito, Scheme 3) [12].

SSH-Mito is a TP ratiometric probe based on the internal charge transfer (ICT) process [31]. The emission spectra of SSH-Mito showed a gradual increase at 525–$575\,$nm (F_{yellow}) with a concomitant decrease at 425–475 (F_{blue}) nm in the presence of $10\,$mM GSH in MOPS buffer ($30\,$mM, pH 7.4) (Table 1). The reaction followed 2nd-order kinetics with k_2 = 2.3×10^{-2} $M^{-1}\,s^{-1}$ (Scheme 3) [12]. This indicates that the reaction proceeds by the rate-limiting attack of GSH at the disulfide bond followed by the cleavage of the C-N bond to afford **1**-SSH (Scheme 3). SSH-Mito exhibited strong response toward thiols, including GSH, Cys, dithiothreitol (DTT), 2-mercaptoethanol (2-ME), and 2-aminoethanethiol (2-AET), and a negligible response toward amino acids without thiol groups (glu, ser, val, met, ala, and ile), metal ions (Na^+, K^+, Ca^{2+}, Mg^{2+}, and Zn^{2+}), and H_2O_2 and was pH insensitive at the biologically relevant pH range [19]. Moreover, F_{yellow}/F_{blue}, the ratio of the intensities at 425–$475\,$nm (F_{blue}) and 525–$575\,$nm (F_{yellow}), increased by 45-fold in the presence of $10\,$mM GSH (Table 1). Further, the TP action spectra of SSH-Mito and **1**-SSH indicate $\Phi\delta_{max}$ values of 80 and 55 GM at 740 and 750 nm, respectively, which are comparable to those of existing TP probes (Table 1) [15]. These results predict a bright ratiometric TPM image of the living specimens stained with SSH-Mito.

SSH-Mito was found to locate predominantly in mitochondria as revealed by the colocalization experiment with MitoTracker Red ($A = 0.85$) [12]. Upon 740 nm TP excitat-

ion, the ratio image of the SSH-Mito-labeled HeLa cells, constructed from two collection windows, gave an average emission ratio of 1.24 (Figures 5(a) and 5(e)). More importantly, SSH-Mito was responsive to the changes in the thiol concentration; the F_{yellow}/F_{blue} ratio increased to 2.64 when the cells were preincubated for 1 day with α-lipoic acid (Figure 5(b)), which increases GSH production [49], and the value was nearly identical to those obtained with **1**-SSH (2.73, Figure 5(d)). The F_{yellow}/F_{blue} ratio also decreased to 0.77 upon treatment with N-ethylmaleimide (NEM) (Figure 5(c)), a well-known thiol-blocking reagent [50]. Further, SSH-Mito is nontoxic to cells during the imaging experiments as determined by a CCK-8 kit. These results establish that SSH-Mito is capable of detecting mitochondrial thiol in the live cells.

The TPM image of fresh hippocampal slices from a 14-day-old rat labeled with $20\,\mu$M SSH-Mito revealed that thiols are more or less evenly distributed in both CA1 and CA3 regions at depths of 90–$190\,\mu$m (Figure 6(b)). Moreover, the image at a higher magnification clearly shows the thiol distribution in the individual cells in the CA1 region with an average emission ratio of 1.66 at a $120\,\mu$m depth (Figure 6(c)). Upon treatment of the tissue with $100\,\mu$M NEM for 30 min, the ratio decreased to 0.85 (Figure 6(f)). It is worth noting that the changes in the emission ratios measured deep inside the tissue slice are comparable to those in the cells. Hence, SSH-Mito is clearly capable of detecting mitochondrial thiols in live tissues using TPM [12].

5. Conclusions

We have developed a series of mitochondrial-targeted TP probes that can selectively detect the Zn^{2+}, H_2O_2, and thiols, respectively, in live cells and tissues. All of these probes have been developed by linking mitochondrial targeting site and specific receptors at the opposite ends of the TP fluorophore. They show significant TP action cross-sections, a marked turn-on or ratiometric response upon reaction with the analytes, good mitochondrial localization, low cytotoxicity, insensitivity to pH in the biologically relevant pH range, and can visualize the distribution and changes in mitochondrial Zn^{2+}, H_2O_2, and thiols levels, respectively, in live tissues at more than $100\,\mu$m depth by TPM without interference from other biologically relevant species.

Acknowledgments

References

[1] J. F. Turrens, "Mitochondrial formation of reactive oxygen species," *The Journal of Physiology*, vol. 552, part 2, pp. 335–344, 2003.

[2] B. C. Dickinson and C. J. Chang, "Chemistry and biology of reactive oxygen species in signaling or stress responses," *Nature Chemical Biology*, vol. 7, no. 8, pp. 504–511, 2011.

[3] Z. A. Wood, E. Schröder, J. Robin Harris, and L. B. Poole, "Structure, mechanism and regulation of peroxiredoxins," *Trends in Biochemical Sciences*, vol. 28, no. 1, pp. 32–40, 2003.

[4] R. Carmel and D. W. Jacobsen, Eds., *Homocysteine in Health and Disease*, Cambridge University Press, Cambridge, UK, 2001.

[5] T. P. Dalton, H. G. Shertzer, and A. Puga, "Regulation of gene expression by reactive oxygen," *Annual Review of Pharmacology and Toxicology*, vol. 39, pp. 67–101, 1999.

[6] M. Marí, A. Morales, A. Colell, C. García-Ruiz, and J. C. Fernández-Checa, "Mitochondrial glutathione, a key survival antioxidant," *Antioxidants & Redox Signaling*, vol. 11, no. 11, pp. 2685–2700, 2009.

[7] S. L. Sensi, D. Ton-That, J. H. Weiss, A. Rothe, and K. R. Gee, "A new mitochondrial fluorescent zinc sensor," *Cell Calcium*, vol. 34, no. 3, pp. 281–284, 2003.

[8] R. P. Haugland, Ed., *A Guide to Fluorescent Probes and Labeling Technologies*, Molecular Probes, Eugene, Ore, USA, 10th edition, 2005.

[9] B. C. Dickinson and C. J. Chang, "A targetable fluorescent probe for imaging hydrogen peroxide in the mitochondria of living cells," *Journal of the American Chemical Society*, vol. 130, no. 30, pp. 9638–9639, 2008.

[10] N. Y. Baek, C. H. Heo, C. S. Lim et al., "A highly sensitive two-photon fluorescent probe for mitochondrial zinc ions in living tissue," *Chemical Communications*, vol. 48, no. 38, pp. 4546–4548, 2012.

[11] G. Masanta, C. H. Heo, C. S. Lim et al., "A mitochondria-localized two-photon fluorescent probe for ratiometric imaging of hydrogen peroxide in live tissue," *Chemical Communications*, vol. 48, no. 29, pp. 3518–3520, 2012.

[12] C. S. Lim, G. Masanta, H. J. Kim, J. H. Han, H. M. Kim, and B. R. Cho, "Ratiometric detection of mitochondrial thiols with a two-photon fluorescent probe," *Journal of the American Chemical Society*, vol. 133, no. 29, pp. 11132–11135, 2011.

[13] F. Helmchen and W. Denk, "Deep tissue two-photon microscopy," *Nature Methods*, vol. 2, no. 12, pp. 932–940, 2005.

[14] W. R. Zipfel, R. M. Williams, and W. W. Webb, "Nonlinear magic: multiphoton microscopy in the biosciences," *Nature Biotechnology*, vol. 21, no. 11, pp. 1369–1377, 2003.

[15] H. M. Kim and B. R. Cho, "Two-photon probes for intracellular free metal ions, acidic vesicles, and lipid rafts in live tissues," *Accounts of Chemical Research*, vol. 42, no. 7, pp. 863–872, 2009.

[16] H. M. Kim and B. R. Cho, "Two-photon fluorescent probes for metal ions," *Chemistry*, vol. 6, no. 1, pp. 58–69, 2011.

[17] R. M. Williams, W. R. Zipfel, and W. W. Webb, "Multiphoton microscopy in biological research," *Current Opinion in Chemical Biology*, vol. 5, no. 5, pp. 603–608, 2001.

[18] C. Xu, W. Zipfel, J. B. Shear, R. M. Williams, and W. W. Webb, "Multiphoton fluorescence excitation: new spectral windows for biological nonlinear microscopy," *Proceedings of the National Academy of Sciences of the United States of America*, vol. 93, no. 20, pp. 10763–10768, 1996.

[19] G. Masanta, C. S. Lim, H. J. Kim, J. H. Han, H. M. Kim, and B. R. Cho, "A mitochondrial-targeted two-photon probe for zinc ion," *Journal of the American Chemical Society*, vol. 133, no. 15, pp. 5698–5700, 2011.

[20] M. P. Murphy and R. A. J. Smith, "Targeting antioxidants to mitochondria by conjugation to lipophilic cations," *Annual Review of Pharmacology and Toxicology*, vol. 47, pp. 629–656, 2007.

[21] L. F. Yousif, K. M. Stewart, and S. O. Kelley, "Targeting mitochondria with organelle-specific compounds: strategies and applications," *ChemBioChem*, vol. 10, no. 12, pp. 1939–1950, 2009.

[22] B. L. Vallee and K. H. Falchuk, "The biochemical basis of zinc physiology," *Physiological Reviews*, vol. 73, no. 1, pp. 79–118, 1993.

[23] J. M. Berg and Y. Shi, "The galvanization of biology: a growing appreciation for the roles of zinc," *Science*, vol. 271, no. 5252, pp. 1081–1085, 1996.

[24] C. J. Frederickson, J. Y. Koh, and A. I. Bush, "The neurobiology of zinc in health and disease," *Nature Reviews Neuroscience*, vol. 6, no. 6, pp. 449–462, 2005.

[25] S. Y. Assaf and S. H. Chung, "Release of endogenous Zn^{2+} from brain tissue during activity," *Nature*, vol. 308, no. 5961, pp. 734–736, 1984.

[26] G. A. Howell, M. G. Welch, and C. J. Frederickson, "Stimulation-induced uptake and release of zinc in hippocampal slices," *Nature*, vol. 308, no. 5961, pp. 736–738, 1984.

[27] S. L. Sensi, H. Z. Yin, and J. H. Weiss, "AMPA/kainate receptor-triggered Zn^{2+} entry into cortical neurons induces mitochondrial Zn^{2+} uptake and persistent mitochondrial dysfunction," *European Journal of Neuroscience*, vol. 12, no. 10, pp. 3813–3818, 2000.

[28] S. L. Sensi, P. Paoletti, A. I. Bush, and I. Sekler, "Zinc in the physiology and pathology of the CNS," *Nature Reviews Neuroscience*, vol. 10, no. 11, pp. 780–791, 2009.

[29] H. M. Kim, M. S. Seo, M. J. An et al., "Two-photon fluorescent probes for intracellular free zinc ions in living tissue," *Angewandte Chemie*, vol. 47, no. 28, pp. 5167–5170, 2008.

[30] K. Komatsu, K. Kikuchi, H. Kojima, Y. Urano, and T. Nagano, "Selective zinc sensor molecules with various affinities for Zn^{2+}, revealing dynamics and regional distribution of synaptically released Zn^{2+} in hippocampal slices," *Journal of the American Chemical Society*, vol. 127, no. 29, pp. 10197–10204, 2005.

[31] A. P. de Silva, H. Q. N. Gunaratne, T. Gunnlaugsson et al., "Signaling recognition events with fluorescent sensors and switches," *Chemical Reviews*, vol. 97, no. 5, pp. 1515–1566, 1997.

[32] E. U. Akkaya, M. E. Huston, and A. W. Czarnik, "Chelation-enhanced fluorescence of anthrylazamacrocycle conjugate probes in aqueous solution," *Journal of the American Chemical Society*, vol. 112, no. 9, pp. 3590–3593, 1990.

[33] T. D. Rae, P. J. Schmidt, R. A. Pufahl, V. C. Culotta, and T. V. O'Halloran, "Undetectable intracellular free copper: the requirement of a copper chaperone for superoxide dismutase," *Science*, vol. 284, no. 5415, pp. 805–808, 1999.

[34] K. Emmerson and K. Roehrig, "Epidermal growth factor (EGF) stimulation of ATP citrate lyase activity in isolated rat hepatocytes is age dependent," *Comparative Biochemistry and Physiology B*, vol. 103, no. 3, pp. 663–667, 1992.

[35] S. L. Sensi, D. Ton-That, P. G. Sullivan et al., "Modulation of mitochondrial function by endogenous Zn^{2+} pools," *Proceedings of the National Academy of Sciences of the United States of America*, vol. 100, no. 10, pp. 6157–6162, 2003.

[36] E. Aizenman, A. K. Stout, K. A. Hartnett, K. E. Dineley, B. McLaughlin, and I. J. Reynolds, "Induction of neuronal apoptosis by thiol oxidation: putative role of intracellular zinc release," *Journal of Neurochemistry*, vol. 75, no. 5, pp. 1878–1888, 2000.

[37] T. Caporale, D. Ciavardelli, C. Di Ilio, P. Lanuti, D. Drago, and S. L. Sensi, "Ratiometric-pericam-mt, a novel tool to evaluate intramitochondrial zinc," *Experimental Neurology*, vol. 218, no. 2, pp. 228–234, 2009.

[38] D. Harman, "The aging process," *Proceedings of the National Academy of Sciences of the United States of America*, vol. 78, no. 11, pp. 7124–7128, 1981.

[39] T. Finkel and N. J. Holbrook, "Oxidants, oxidative stress and the biology of ageing," *Nature*, vol. 408, no. 6809, pp. 239–247, 2000.

[40] E. R. Stadtman, "Protein oxidation and aging," *Free Radical Research*, vol. 40, no. 12, pp. 1250–1258, 2006.

[41] E. A. Veal, A. M. Day, and B. A. Morgan, "Hydrogen peroxide sensing and signaling," *Molecular Cell*, vol. 26, no. 1, pp. 1–14, 2007.

[42] T. Finkel, M. Serrano, and M. A. Blasco, "The common biology of cancer and ageing," *Nature*, vol. 448, no. 7155, pp. 767–774, 2007.

[43] K. J. Barnham, C. L. Masters, and A. I. Bush, "Neurodegenerative diseases and oxidatives stress," *Nature Reviews Drug Discovery*, vol. 3, no. 3, pp. 205–214, 2004.

[44] M. T. Lin and M. F. Beal, "Mitochondrial dysfunction and oxidative stress in neurodegenerative diseases," *Nature*, vol. 443, no. 7113, pp. 787–795, 2006.

[45] K. M. Geraghty, S. Chen, J. E. Harthill et al., "Regulation of multisite phosphorylation and 14-3-3 binding of AS160 in response to IGF-1, EGF, PMA and AICAR," *Biochemical Journal*, vol. 407, no. 2, pp. 231–241, 2007.

[46] R. Kizek, J. Vacek, L. Trnková, and F. Jelen, "Cyclic voltammetric study of the redox system of glutathione using the disulfide bond reductant tris(2-carboxyethyl)phosphine," *Bioelectrochemistry*, vol. 63, no. 1-2, pp. 19–24, 2004.

[47] M. Marí, A. Morales, A. Colell, C. García-Ruiz, and J. C. Fernández-Checa, "Mitochondrial glutathione, a key survival antioxidant," *Antioxidants and Redox Signaling*, vol. 11, no. 11, pp. 2685–2700, 2009.

[48] F. Q. Schafer and G. R. Buettner, "Redox environment of the cell as viewed through the redox state of the glutathione disulfide/glutathione couple," *Free Radical Biology and Medicine*, vol. 30, no. 11, pp. 1191–1212, 2001.

[49] B. Hultberg, A. Andersson, and A. Isaksson, "Lipoic acid increases glutathione production and enhances the effect of mercury in human cell lines," *Toxicology*, vol. 175, no. 1–3, pp. 103–110, 2002.

[50] C. R. Yellaturu, M. Bhanoori, I. Neeli, and G. N. Rao, "*N*-Ethylmaleimide inhibits platelet-derived growth factor BB-stimulated Akt phosphorylation via activation of protein phosphatase 2A," *The Journal of Biological Chemistry*, vol. 277, no. 42, pp. 40148–40155, 2002.